Journal of Crystal Growth 430 (2015) 21–27

Contents lists available at ScienceDirect

Journal of Crystal Growth

journal homepage: www.elsevier.com/locate/jcrysgro

Principles of electroless photoetching of non-uniformly doped GaN: Kinetics and defect revealing

J.L. Weyher [a,*], D.H. van Dorp [b], J.J. Kelly [c]

[a] Institute of High Pressure Physics, Polish Academy of Sciences, ul. Sokołowska 29/37, 01-142 Warsaw, Poland
[b] Imec, Surface and Interface Processing, Kapeldreef 75, B-3001 Leuven, Belgium
[c] Condensed Matter and Interfaces, Debye Institute for NanoMaterials Science, University of Utrecht, Princetonplein 1, Utrecht, The Netherlands

ARTICLE INFO

Article history:
Received 24 June 2015
Received in revised form
30 July 2015
Accepted 7 August 2015
Communicated by: Dr. T. Paskova
Available online 20 August 2015

Keywords:
A1. Crystal structure
B1. Nitrides
Etching

ABSTRACT

When using electroless etching of semiconductors for quality control or device applications one must be aware of the possibility of galvanic interaction in the system. Here we show how highly doped (n^{++}) GaN in a bilayer heterostructure dramatically increases the photoetch rate of the low doped (n) GaN layer in alkaline peroxydisulphate solution (the n^{++} material does not etch). Contacting the bilayer to a platinum sheet in solution further increases the photoetch rate. We show how previous electrochemical studies on GaN can be used to understand such "galvanic" effects. The present results offer an explanation for unexpected features in the photoetching of compound semiconductors which, during growth, become non-uniformly doped either by accident or by design. The work describes an example of the former case: non-uniformity due to the formation of extended defects, e.g. overgrown pinholes in GaN. The relevance of this study for practical applications, including the revealing of crystallographic defects for quality control, is considered.

1. Introduction

Electroless etching, widely used in semiconductor device technology, has the advantage that, unlike electrochemical etching, it does not require an Ohmic contact to the sample or an external voltage source [1–6]. Electroless etching is based on two electrochemical reactions. An oxidizing agent (an electron acceptor) in solution is reduced by extraction of electrons from the valence band (VB) of the solid; this is equivalent to the injection of holes into the band. The holes, localized in surface bonds, serve to oxidize the semiconductor; the surface bonds are broken, resulting in etching. In electroless photoetching, the subject of the present paper, supra-bandgap light is used to generate electron–hole pairs. The conduction band (CB) electrons are captured by the oxidizing agent while the valence band holes cause dissolution of the semiconductor [1,7,8]. Since electrons and holes are mobile charge carriers the two partial reactions, oxidation and reduction, can be spatially separated. For example, in the photoetching of n-type samples the etch rate can be enhanced by short-circuiting the semiconductor to a catalytically active metal such as Pt; the photogenerated electrons pass to the metal where they react more effectively with the oxidizing agent [1,8–11]. This combination of metal and semiconductor is, in fact, a galvanic element or cell: the semiconductor acts as cathode and the metal as anode. Consequently, this form of photoetching involving an auxiliary electrode (but no voltage source) is termed "photogalvanic" [1]. The semiconductor and metal may be in direct electrical contact, e.g. with a metal layer on the semiconductor [2,4–6,12,13]. Galvanic effects can also be observed when the semiconductor forms part of a heterojunction, e.g. as in a p/n junction [14].

The technologically important semiconductor GaN can be etched electrochemically, i.e. in a cell containing an electrolyte solution and a counter electrode, with the reaction driven by a voltage source [15]. The p-type material is etched in the dark while n-type requires illumination to generate VB holes. Because of its deep-lying VB edge, injection of holes from an oxidizing agent in solution is, under normal conditions, not possible, thus precluding electroless etching in the dark. Minsky et al. [9] have shown that photogalvanic etching of GaN is possible in alkaline solution. They and others have used this approach for various applications: quality control based on defect revealing, surface treatment and polishing, and pattern definition [10,11,16–20]. Macht and coworkers [21] showed that such photogalvanic etching is made possible by gaseous oxygen normally present in aqueous solution. Oxygen acts as an acceptor of CB electrons, though only at a significant rate with the aid of an auxiliary electrode. The discovery that addition of the peroxydisulphate anion $\left(S_2O_8^{2-}\right)$ to the alkaline solution increases the photogalvanic etch rate markedly and even enables electroless photoetching in certain cases [12,22] was an important development.

* Corresponding author.
E-mail address: weyher@unipress.waw.pl (J.L. Weyher).

http://dx.doi.org/10.1016/j.jcrysgro.2015.08.003
0022-0248/

In this work we consider the photoetching of non-uniformly doped n-type GaN crystals and GaN heterostructures in peroxydisulphate solution. The work was inspired by previous studies of the compound semiconductors, GaAs, GaN and SiC, that revealed a number of interesting features [23,24]. Results for GaN, shown in Fig. 1, are typical for these materials. The photoetch rate R is plotted as a function of the free carrier concentration n (on a logarithmic scale) for two HVPE-grown samples. Three trends are clear: (1) higher photogalvanic etch rates R are observed at areas with lower carrier concentration n; (2) plots of R versus $\ln(n)$ are linear ($R=-\beta\ln(n/n_0)$) where β is the slope and n_0 corresponds to the $R=0$ intercept on the n-axis; (3) plots of R versus $\ln(n)$ for samples cut from different crystals are parallel with a sample-specific shift [23]. The latter feature indicates that the etch rate of areas with the same carrier density (e.g. 5×10^{17} cm^{-3} in Fig. 1) from different samples may differ considerably (R_1 and R_2 in the figure).

To check the possibility that galvanic interaction between regions of different dopant density might be responsible for these results, bilayer samples of n-type GaN were prepared, consisting of two well-defined layers with markedly different but macroscopically uniform carrier density. In this paper we describe the results of photoetching of such samples, as well as some results for GaN grown by MOCVD on sapphire. Electroless (photo)etching can be considered a form of electrochemical etching in which charge carriers are supplied directly to the dissolving surface by a species in solution instead of from a counter electrode via a voltage source [1]. Previously we have reported on the photoelectrochemistry of n-type GaN in alkaline solution [21,22] and the results of these studies form the basis for an interpretation of the present results. We show that galvanic interaction can account qualitatively for the photoetching of both heterostructures and non-uniformly doped crystals. The consequences of these results for defect revealing are considered.

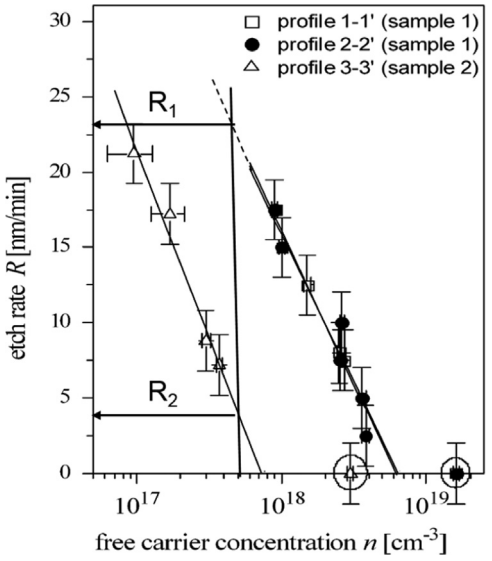

Fig. 1. Plots of the photogalvanic etch rate R as a function of the local free-carrier concentration n for two different non-uniformly doped HVPE-grown GaN samples (n was determined by Raman spectroscopy). R_1 and R_2 represent etch rates for two regions with the same free-carrier concentration (5×10^{17} cm^{-3}) in the different samples. The slightly modified figure is reprinted with permission from Ref. [23].

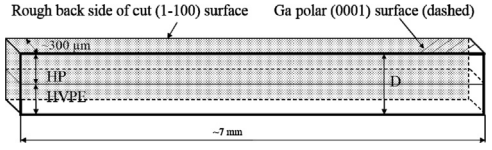

Fig. 2. The geometry of the HVPE/HP GaN bilayer heterostructures used in this study. The bold rectangle shows the $(1\bar{1}00)$ surface that was cut, polished and subjected to RIE prior to photoetching. The type A and B samples had an initial thickness D of approximately 900 and 430 µm, respectively.

2. Experimental

2.1. Materials

In this study special heterostructures were used: bilayers cut from crystals of High Pressure (HP) GaN grown on a Hydride Vapor Phase Epitaxy (HVPE) GaN template, using the multi-feed seed (MFS) method. Details of the growth conditions are reported elsewhere [25]. Two combinations of HP and HVPE material, both n-type, were used. In both, the HP carrier density n was 5×10^{19} cm^{-3}. In the first combination (type A) the HVPE carrier density was 1×10^{17} cm^{-3}, in the second (type B) it was 5×10^{16} cm^{-3}. The carrier density was determined by the Van der Pauw method. SIMS measurements revealed that oxygen was the main contaminating element responsible for the n-type properties of HVPE-grown crystals (non-intentional doping) and for the high electron density in the HP-grown material [26].

The HVPE/HP crystals were cut along the $(1\bar{1}00)$ plane into a number of beams with an initial thickness D, a width of 300 µm and a length of approximately 7 mm (see Fig. 2). This face is widely used because it is an easy cleaving plane (see also Fig. 8(a)) with, as for the samples used here, a low dislocation density. To obtain the desired HVPE/HP thickness ratio the samples were thinned. Prior to photoetching one $(1\bar{1}00)$ face was polished and work damage was removed by reactive ion etching (RIE). In the type A samples ($D=870$ µm; $n=1\times10^{17}$ cm^{-3}) two different HVPE/HP thickness ratios were used: 6/4 and 5/5 (see Fig. 3(c) and (d)). In addition two reference samples consisting of either HP (Fig. 3(a)) or HVPE material (Fig. 3(b)) were obtained by thinning the original beams. All type A samples were mounted together on a glass plate with wax so that only the polished $(1\bar{1}00)$ surface was exposed to the solution. The type B samples ($D=430$ µm; $n=5\times10^{16}$ cm^{-3}) had a HVPE/HP thickness ratio of 5/5 (each layer was 180 µm thick). These samples were used to investigate, in addition, the influence of contact of the GaN bilayer to an auxiliary Pt electrode. The etching

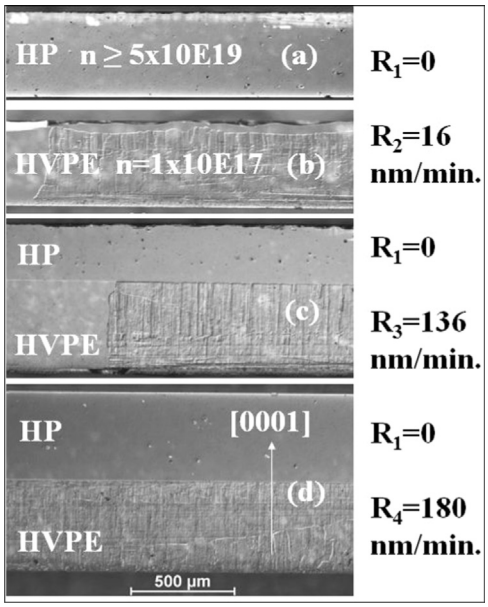

Fig. 3. DIC optical images of photoetched $(1\bar{1}00)$ sections from MFS-grown GaN: (a) HP only; (b) HVPE only; (c) and (d) refer to HVPE/HP bilayers with thickness ratio 6/4 and 5/5, respectively. The corresponding etch rates are shown.

geometry of these samples will be described in the Results section. A third type of sample was also investigated: a 5 μm thick Si-doped GaN layer grown by MOCVD on sapphire. The carrier density in this material was 1×10^{18} cm^{-3}. Samples 5×5 mm, cut from the 3-in. wafer, were used to study defects in the Ga-polar surface by photoetching in both electroless and galvanic modes.

2.2. Photoetching

Electroless photoetching was performed with a 0.02 M $K_2S_2O_8$, 0.02 M KOH solution (designated KSO-D solution in previous papers [27,28]) using a 300 W UV-enhanced Xe lamp (Oriel). This method was developed for the rapid revealing and analysis of dislocations and electrically active inhomogeneities in epitaxial and bulk GaN crystals [28–30]. For photogalvanic etching the GaN sample was connected to a Pt electrode (area approximately 2 cm^2) by using a Ti spring as contact to the semiconductor (surprizingly this gives a good electrical contact to higher doped GaN in peroxydisulphate solution). The current passing between GaN and Pt could be measured with an ammeter. After etching, the samples were examined by differential interference contrast (DIC) microscopy and scanning electron microscopy (SEM). For etch rate measurements part of the sample surface was masked by wax. After removal of the wax, the etched depth was determined with a Tencor Alfa Step profiler.

3. Results and discussion

3.1. Galvanic interaction in photoetching of heterostructures

Results for the photoetching of type A samples in which only the polished $(1\bar{1}00)$ face was exposed to solution are given in Fig. 3. The two reference samples, only HP and only HVPE, show a considerable difference in etching properties: the photoetch rate of the low-doped HVPE sample (b) was 16 nm min^{-1} while that of the high-doped HP sample (a) was too low to be measured. The HVPE etch rate in the bilayer sample (c) with a HVPE/HP thickness ratio of 6/4 was increased by almost an order of magnitude (to 136 nm min^{-1}) compared to that of the reference sample (b). This indicates that, although the HP material is not etching, it influences markedly the HVPE photoetch rate. The increase in dissolution rate of sample (d) with a thickness ratio of 5/5 (to 180 nm min^{-1}) suggests that the area ratio of the high and low-doped materials exposed to the solution may be important. Again, in this case the HP layer was not etched.

To understand the results shown in Fig. 3 we first consider the processes involved in the photoetching of n-type GaN in $S_2O_8^{2-}$/KOH solution using a band-energy diagram of the semiconductor (see inset Fig. 4). Step (1) involves the generation of an electron in the conduction band (CB) and hole in the valence band (VB) by a supra-bandgap photon

$$h\nu \rightarrow e^-(CB) + h^+(VB) \quad (1)$$

The majority carriers, electrons, are captured by the $S_2O_8^{2-}$ anion [22] leading to its reduction to sulfate, SO_4^{2-} (step (2)).

$$S_2O_8^{2-} + 2e^- \rightarrow 2SO_4^{2-} \quad (2)$$

(That this reaction is more complex than indicated in Eq. (2) and Fig. 4 [22] is not important for the present discussion.) The minority carriers, holes, are used for oxidation (etching) of the semiconductor (step (3)).

$$GaN + 6OH^- + 3h^+ \rightarrow GaO_3^{3-} + 3H_2O + 1/2N_2 \quad (3)$$

Three holes are required to photoetch one formula-unit of GaN; a gallate ion in solution and gaseous nitrogen are formed [22]. The charge transfer reactions (2) and (3) must compete with recombination of electrons from the conduction band with holes from the valence band (step (1)). In the steady state the rate of transfer of electrons and holes to solution must be equal, i.e. the rates of reduction of $S_2O_8^{2-}$ (Eq. (2)) and oxidation of GaN (Eq. (3)) are charge-balanced. Steps (2) and (3) are electrochemical reactions whose rates can be varied by applying a potential to the semiconductor. This can be achieved by connecting the GaN sample to a counter electrode (e.g. Pt) via a voltage source in an electrochemical cell and measuring the current in the external circuit as a function of applied potential U [1,15]. The steps (2) and (3) can be studied separately in two experiments.

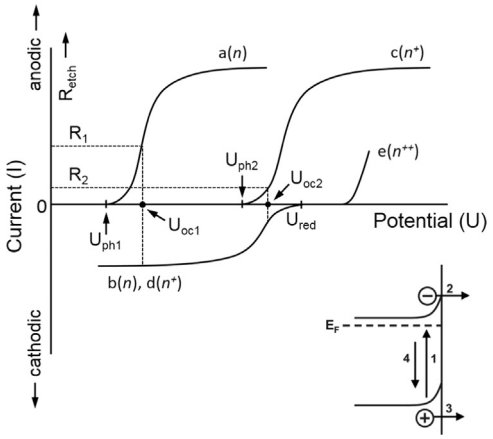

Fig. 4. The inset shows a schematic energy band diagram giving the steps involved in electroless photoetching (for details: see the text). The main figure shows schematically the potential dependence of (i) the photocurrent measured during *anodic* dissolution of n, n^+ and n^{++} GaN in KOH solution (curves (a), (c) and (e), respectively) and (ii) the *cathodic* current due to reduction of $S_2O_8^{2-}$ in KOH solution at n and n^+ GaN in the dark (curves (b) and (d), respectively). Electroless photoetching occurs at the open-circuit potential (U_{OC1} and U_{OC2} for n and n^+, respectively) at which anodic and cathodic current are equal ($I_{total}=0$). The corresponding etch rates (R_1, R_2) are shown.

To study the oxidation and dissolution of GaN (Eq. (3)) a KOH solution without $S_2O_8^{2-}$ is used. This reaction requires VB holes, minority carriers that must be generated by light. In an electrochemical experiment, majority carriers (electrons) flow to the counter electrode, giving rise to an "anodic" photocurrent in the external circuit. The corresponding current–potential curve is shown as (a) in Fig. 4. Before the onset of photocurrent at U_{ph1} photogenerated electrons and holes recombine; in this range the concentration of majority carriers is high. As the potential is made positive with respect to U_{ph1} the surface electron concentration decreases. The electric field of the depletion layer separates the electrons and holes. The holes are driven to the surface by the field and by diffusion; the electrons pass to the counter electrode. The resulting anodic photocurrent increases with increasing potential, i.e. the etch rate R_{etch} increases (see Eq. (3)). Finally, all photogenerated holes reach the surface where they react, giving rise to a constant photocurrent, i.e. constant R_{etch}. Reduction of $S_2O_8^{2-}$ at n-type GaN in KOH solution requires CB electrons, i.e. majority carriers (see Eq. (2)). In an electrochemical experiment its rate can therefore be measured as a *dark* current and is not influenced by light (the electrons are supplied from the counter electrode). The potential dependence of this "cathodic" dark current, with onset at U_{red}, is shown schematically as curve (b) in Fig. 4. The reaction rate increases on going to negative potential, as the electron density in the CB at the surface increases and majority carrier accumulation is reached [22]. At more negative potential the reduction reaction becomes dependent on mass transport of $S_2O_8^{2-}$ to the surface, i.e. its rate becomes constant [22].

In an electrochemical experiment in which the GaN electrode is illuminated in a KOH solution containing $S_2O_8^{2-}$, one measures a

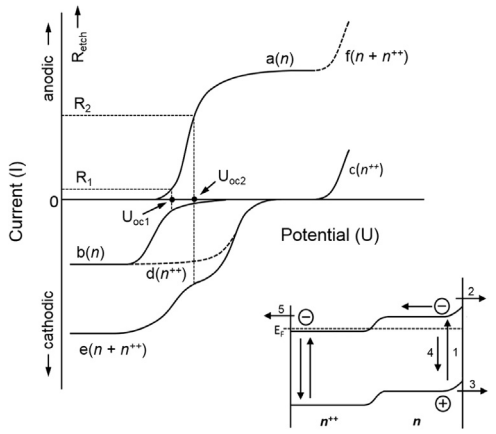

Fig. 5. The inset illustrates galvanic interaction in photoetching of a GaN n/n^{++} heterostructure. Electrons transferred from the n to the n^{++} layer cause reduction of $S_2O_8^{2-}$ at the latter. As a result, electron–hole recombination at the surface of the n layer is reduced and its etch rate is enhanced. The main figure shows the potential dependence of (i) the photocurrent measured during *anodic* dissolution of n and n^{++} GaN in KOH solution (curves (a) and (c), respectively) and (ii) the *cathodic* current due to reduction of $S_2O_8^{2-}$ at n and n^{++} GaN (curves (b) and (d), respectively). Electroless photoetching of the n GaN occurs at U_{OC1}, at a rate R_1 (n^{++} does not etch). When n and n^{++} are in electrical contact the total cathodic current (curve (e) ($n+n^{++}$)) and anodic current (curve (f) ($n+n^{++}$)) determine the open-circuit potential U_{OC2} and the markedly enhanced etch rate R_2.

"total" current–potential plot. The total current, the sum of anodic and cathodic current at each potential, is not shown in Figs. 4 and 5 for the sake of clarity. At open-circuit, with no applied potential and no current flowing between GaN and Pt, the anodic current must be equal to the cathodic current ($I_{total}=0$), i.e. the rates of oxidation of GaN and reduction of $S_2O_8^{2-}$ must be charge-balanced. This condition defines the open circuit or rest potential of the system U_{oc1} and, consequently, the open-circuit etch rate R_1, as observed during electroless photoetching.

Previous work has shown that the onset of anodic photocurrent shifts to positive potential as the dopant density is increased in the range from moderate ($n \sim 10^{17}$ cm^{-3}) to high ($n^+ \sim 5\times10^{18}$ cm^{-3}) [21]. This trend is mainly due to enhanced carrier recombination as a result of a decrease in minority carrier diffusion length and space charge layer thickness. The result is shown schematically in Fig. 4 for moderately doped (n) and higher doped (n^+) GaN, curves (a) and (c), respectively. In this range the influence of dopant density on the cathodic current is limited: curve (d) for the n^+ electrode is shown the same as curve (b) for the lower doped electrode (we assume that the GaN area is the same for both cases). From Fig. 4 curves (c) and (d) it is clear that the open-circuit potential for the higher doped GaN U_{oc2} is at a more positive potential and, as a result, the photoetch rate R_2 has decreased with respect to that of the lower doped sample R_1. If the onset potential for anodic photocurrent is more positive than that of the cathodic current U_{red} (curve (e), n^{++}), electroless photoetching is no longer possible (all photogenerated electrons and holes recombine at open circuit). This is very likely the case for the very highly doped HP material (5×10^{19}/cm^{-3}) used in this study. The difference in onset potential for photocurrent for n and n^+ GaN (curves (a) and (c), Fig. 4) has been exaggerated somewhat to make clearer the effects involved.

To consider the photoetching of bilayer heterostructures consisting of very high-doped (HP and low-doped (HVPE)) materials as in Fig. 3 we use a simplified band diagram in which the two layers are back-to-back (inset Fig. 5). As in the case of low-doped GaN (see Fig. 4) some of the photogenerated holes in the HVPE layer will contribute to photoetching while the remainder will recombine. On the other hand, the charge transfer reactions (2) and (3) cannot compete with recombination in the HP layer: no etching occurs. Since, on illumination, the majority carriers in the system rapidly equilibrate, electrons from the low-doped layer end up at the surface of the high-doped material where they can contribute to reduction of $S_2O_8^{2-}$. This electron transfer from HVPE to HP reduces electron–hole recombination in the HVPE layer and, consequently, the rate of electroless photoetching is increased. The energy barrier between the HP and HVPE layers in Fig. 5 results from the difference in Fermi level E_F due to the considerable difference in dopant density of the two materials.

These steps can also be represented electrochemically. The current–potential curves for a moderately doped HVPE sample (electron density: n) are shown as (a) and (b) in Fig. 5. The photoetch rate at open-circuit potential U_{oc1} is denoted by R_1. Photoanodic oxidation of HP GaN (n^{++}) is shown as curve (c). Clearly, electroless etching is not possible with this material. The extremely high donor density of the HP layer (5×10^{19} cm^{-3}) means that the electrode is degenerate and thus quasi-metallic. As a result, the rate of reduction of $S_2O_8^{2-}$ is expected to be higher than at a HVPE electrode (curve (d), Fig., 5) until mass transport gives rise to a potential-independent cathodic current (we assume that n and n^{++} areas are the same). When the two materials are in electrical contact, as in the bilayer, we need to consider the total anodic current (curve (f)=(a)+(c)) and the total cathodic current (curve (e)=(b)+(d)) [31]. This leads to a new open-circuit potential U_{oc2} and a markedly increased photoetch rate R_2. If we increase the HP area while keeping the HVPE area constant, the contribution of the high-doped material to the total cathodic current is enhanced (the current at a given potential is directly proportional to the area exposed to solution). This will shift the open-circuit potential to an even more positive value, thus further increasing the photoetch rate. In this way we can understand how contacting a HVPE layer with a HP layer (also in contact with solution) increases the photoetch rate and that the area ratio of the two surfaces determines the magnitude of the increase, reported in Fig. 3(c) and (d). As in the case of an n-GaN/metal contact [21,22], a combination of HP/HVPE GaN also acts as a photogalvanic element, with electrons passing from the HVPE to the HP surface.

Using reasoning similar to that described above it is possible to predict the etching result when a bilayer is formed of n and n^+ GaN with the characteristics shown in Fig. 4. The photoetch rate of the lower-doped material will be increased by a factor of approximately two while that of the n^+ layer will be decreased to a low value. If the difference in U_{ph} between n and n^+ is smaller than shown in Fig. 4, the increase in etch rate of n and decrease in etch rate of n^+ will be less pronounced.

3.2. Influence of an auxiliary electrode on photoetching

Type B samples with carrier densities of 5×10^{16} cm^{-3} and 5×10^{19} cm^{-3} for HVPE and HP layers, respectively, were used for experiments similar to those described above for type A samples (Fig. 3(c) and (d)). In addition, the effect of connecting the sample via a Ti contact and wire to an auxiliary Pt electrode was also investigated. Results are given in Table 1.

In experiment 1 only the polished HVPE/HP $\left(1\bar{1}00\right)$ bilayer face was exposed to solution (all other faces were masked by wax). Again, the HP layer was not photoetched. The etch rate of the HVPE layer was 185 nm min^{-1} comparable to that of the corresponding A sample (d) with the same thickness ratio. When all surfaces of this sample were exposed to solution (experiment 2, no masking) the etch rate increased considerably to 400 nm min^{-1}. Enhanced $S_2O_8^{2-}$ reduction at the rough HP backside and other exposed faces increases the photoetch rate of the polished HVPE layer.

The results of experiments 1 and 2 in Table 1, Fig. 3(c) and (d) prove that the significant increase in etch rate of HVPE GaN is due to galvanic interaction with HP material: the highly doped HP layer acts as an auxiliary electrode, shifting the open-circuit potential of the system to a more positive value. Experiment 3 in Table 1 shows that

when the masked HVPE/HP bilayer is connected to a Pt electrode, the photoetch rate is further increased (to 550 nm min^{-1}). In this case $S_2O_8^{2-}$ was also reduced at the Pt. A photocurrent of about 180 μA was measured between GaN and Pt (Fig. 6) during such an experiment. This current corresponds to an etch rate of 400 nm min^{-1}. Clearly, reduction of $S_2O_8^{2-}$ occurs at the surface of both the GaN and the Pt, thus contributing to the higher etch rate. When, as in experiment 4 (a bilayer with all surfaces exposed to solution), the GaN was also connected to Pt, the same etch rate was found as for experiment 3 without the auxiliary electrode. This indicates that in these two experiments the open-circuit potential is in the saturation range of the photocurrent, i.e. the photoetch rate is independent of potential.

Table 1

Etch rate of the polished HVPE $\left(1\bar{1}00\right)$ surface of a HVPE/HP bilayer (type B) for different modes of photoetching in 0.02 M $S_2O_8^{2-}$/0.02 M KOH solution (KSO-D standard etchant). For details see the text.

Experiment	Masking	Pt (aux. elec.)	R (nm min^{-1})
#1	Yes	No	185
#2	No	No	400
#3	Yes	Yes	550
#4	No	Yes	550

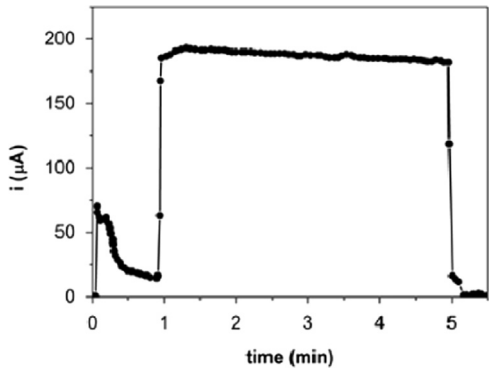

Fig. 6. Short-circuit current measured when a $\left(1\bar{1}00\right)$ HVPE/HP GaN bilayer was connected to a Pt electrode in $S_2O_8^{2-}$/KOH solution. Illumination of the sample was started 1 min after immersion (see experiment #3, Table 1).

The electroless photoetch rate of heteroepitaxial GaN samples grown by MOCVD on sapphire was low. This is to be expected [21,22] since the dopant density is quite high (1×10^{18} cm^{-3}). Connecting the sample to a Pt auxiliary electrode enhanced the photoetch rate significantly. This is the same photogalvanic effect as reported for experiment 3 of Table 1. Photogalvanic etching proved an effective method for revealing dislocations in this material while electroless photoetching was not as effective. Fig. 7 summarizes the results.

With the Pt counter electrode connected to the GaN sample photoetching was fast and reproducible. Nanopillars, formed on threading dislocations, have a well-defined morphology, similar to that obtained with KOH solution containing oxygen [22], i.e. there is a constant diameter along the pillars, even after prolonged etching, as shown in Fig. 7(a) and (b). On the other hand, electroless photoetching (i.e. without the Pt electrode) of samples cut from the same GaN wafer required a long "incubation" time for dissolution (Fig. 7(c)). The etching time needed to reveal dislocations (in this case in the form of conical pyramids, Fig. 7(d)), was more than a factor of 10 longer than for the photogalvanic mode. The conical shape of dislocation-related etch features was not previously observed on numerous GaN samples etched photogalvanically in KOH solution containing O_2 or

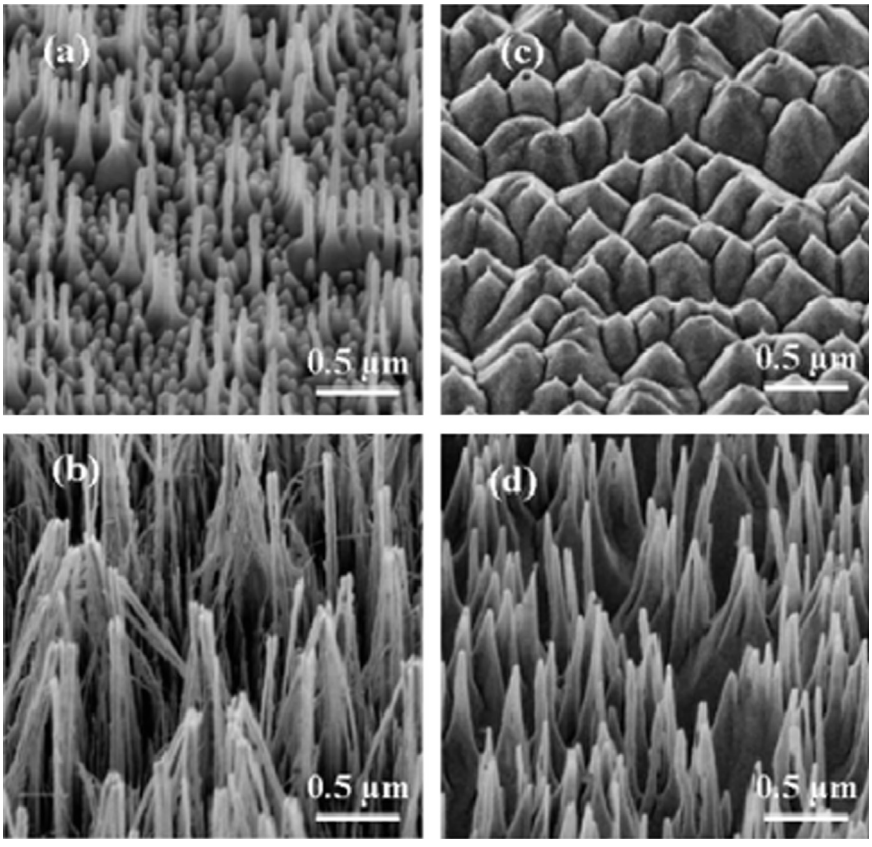

Fig. 7. SEM images of GaN grown by MOCVD on sapphire and photoetched in $S_2O_8^{2-}$/KOH (KSO-D standard solution): (a) and (b) in photogalvanic mode for 5 and 10 min, respectively; (c) and (d) in electroless mode (i.e. without Pt) for 30 and 70 min, respectively.

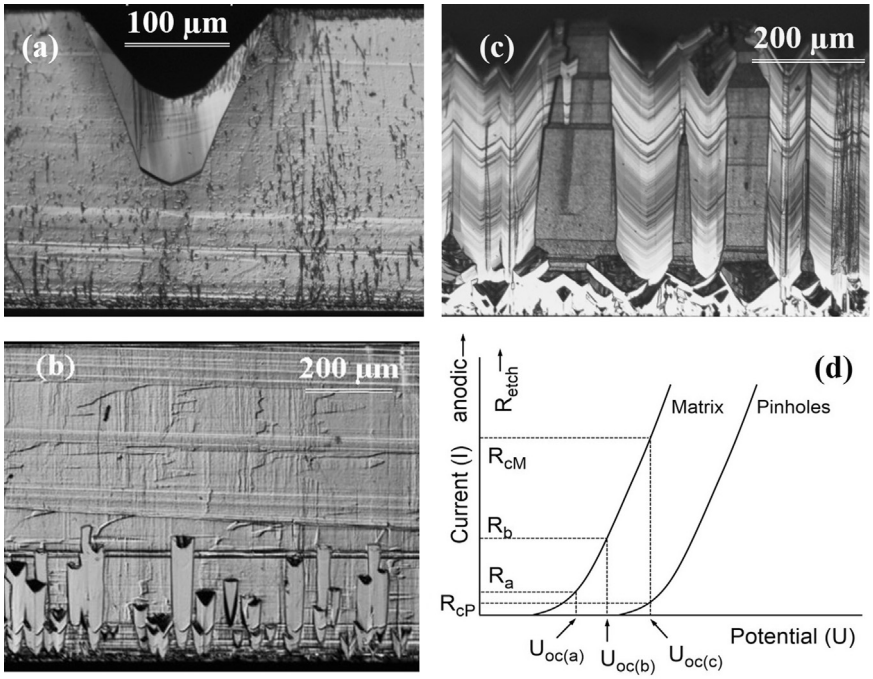

Fig. 8. DIC optical images of $\left(1\bar{1}00\right)$ cross sections of thick HVPE-grown GaN after electroless photoetching (i.e. without a Pt auxiliary electrode). Sample (a) contained a single overgrown pinhole. Samples (b) and (c) contained many such pinholes. The surface coverage by pinholes for samples (a), (b) and (c) was approximately 5%, 20% and 80%, respectively. The electron density of the GaN matrix was 1×10^{17} while that of the overgrown pinhole regions was about 1×10^{19}. (d) Schematic photocurrent/etch rate-potential plots for the two materials, matrix and overgrown pinholes, indicating the open-circuit potential, which is determined by the area ratio of the two materials exposed to solution.

$S_2O_8^{2-}$ [22,32]. In the electroless case the open-circuit potential of samples with a dopant density of 10^{18} cm^{-3} will be close to the onset potential for photocurrent (U_{oc2}, Fig. 4(b)). In this range, electron–hole recombination is more effective than etching and this may retard dissolution of the semiconductor at the pyramid base. Photogalvanic etching of the heteroepitaxial GaN in $S_2O_8^{2-}$/KOH solution has been used to produce uniformly "rough" platforms for surface-enhanced Raman spectroscopy (SERS) applications [33].

3.3. Photoetching of non-uniformly doped semiconductors

On the basis of the current–potential curves shown in Fig. 4 one expects that, in general, the photoetch rate of the n-type GaN will decrease as the dopant density is increased. We have shown that this is the case for the photoetching of GaN (grown by MOCVD on sapphire) in aerated KOH solution [21]. However, the decrease in etch rate was considerably less pronounced than that shown for the non-uniformly doped samples of Fig. 1. In addition, the fact that regions with the same dopant density show, for different crystals, markedly different photoetch rates may seem surprizing. The experiments on heterostructures described above help us to understand the photoetching results for such doped crystals. As in the case of bilayers (Fig. 5) galvanic interaction will influence the local etch rate. Each region makes a contribution to the total anodic current and the total cathodic current. These contributions depend, not only on the dopant density (Fig. 4) but also on the relative surface area of the region exposed to solution (Fig. 5). Under open-circuit photoetching conditions the total anodic current is equal to the total cathodic current (see Fig. 5). This defines the open-circuit potential of the system and thus the photoetch rate of the different regions. As in the bilayer case, the etch rate of the low-doped regions will generally be increased at the expense of more highly doped areas. Since the relative area of regions of different dopant density exposed to solution is important in determining the total current, it is not surprizing that regions with the same dopant density in different samples do not give the same photoetch rate. It is clear that the prediction of local etch rates in such a poorly defined system is not simple.

Experiments performed on HVPE grown GaN crystals which contained overgrown "pinholes" support the hypothesis described above for non-uniformly doped crystals. The $\left(1\bar{1}00\right)$ sections of three different crystals are shown in Fig. 8. In each case the matrix, grown in the [0001] direction, had a carrier density $\leq 1 \times 10^{17}$ while that of the overgrown pinholes was about 1×10^{19} [30,34]. Sample (a) contained a single pinhole, i.e. a pit about 100 μm wide, that was largely filled with GaN. Samples (b) and (c) had many overgrown pinholes; the percentage of the total surface area covered by such pinholes was approximately 20% and 80% for (b) and (c), respectively (for (a) it was less than 5%). Since these are examples of non-uniformly doped materials, one would expect to see an influence of galvanic interaction on the photoetching properties. The etch rate of sample (a) in the present KSO-D solution was low. A considerable etching time (10 min) was necessary to reveal growth striations and other inhomogeneities. The structure of crystal (b) became clear after much shorter etching, though again, as in case (a), the overgrown pinholes themselves were not etched. A still shorter etching time (2 min) was sufficient to reveal clearly striation patterns in both the matrix and the pinholes of sample (c).

Clearly, the pinhole surface with a high carrier density in electrical contact with the matrix and exposed to solution has a strong influence on photoetching, as one would expect on the basis of Fig. 5. The trend in etch rate is determined by the area ratio of the high and low-doped materials: as this increases, the open-circuit potential of the system shifts to a more positive value, increasing the etch rate of the matrix considerably. This trend is illustrated in Fig. 8(d). Schematic photocurrent (etch rate)–potential curves are shown for material corresponding to the low-doped matrix and the filled pinholes. As the pinhole/matrix area ratio is increased on going from (a) to (c) the open-circuit potential changes from $U_{oc(a)}$ to $U_{oc(c)}$. The corresponding etch rates for matrix and pinholes are

indicated on the current axis. R_a, the etch rate of the matrix for case (a), is low. With the shift in open-circuit potential from $U_{oc(a)}$ to $U_{oc(b)}$, this rate increases to R_b and becomes even higher (R_{cM}) in case (c). In the latter case some etching of the highly doped overgrown pinhole (R_{cP}) is expected. The results of Fig. 8 indicate that the etching time in a practical experiment depends markedly on the actual ratio of areas of different carrier density exposed to solution and cannot be predicted a priori.

It should be remarked that, in contrast to the high density of dislocations ($\sim 2\times 10^8\,cm^{-2}$) present in the MOCVD hetero-epitaxial samples shown in Fig. 7, the density of dislocations in the HVPE-grown samples shown in Fig. 8 is at least two orders of magnitude lower and, especially on the $(1\bar{1}00)$ planes, has no influence on the etch rate of the matrix between overgrown pinholes.

4. Conclusions

Two examples of galvanic interaction during photoetching of GaN in $S_2O_8^{2-}$/KOH solution are considered in this paper. These involve: (i) direct contact between HVPE and HP layers of a GaN bilayer heterostructure and (ii) contact between a heterosturcture or an MOCVD grown GaN layer and a Pt auxiliary electrode (via a Ti contact and a metal wire). In both cases the photoetch rate of relatively low-doped HVPE GaN ($n \le 10^{17}\,cm^{-3}$) was enhanced markedly by contact with high doped HP material ($n > 5\times 10^{19}\,cm^{-3}$) or with Pt. A similar enhancement of photoetch rate was observed with an MOCVD GaN/Pt combination. The results can be rationalized on the basis of the electrochemistry of GaN in $S_2O_8^{2-}$/KOH solution.

These results provide an explanation for the exceptionally strong dependence of photoetch rate on local donor density in non-uniformly doped compound semiconductors (GaN, GaAs, SiC). This hypothesis was further confirmed by experiments which show that overgrown pinholes with a high carrier density ($n \approx 10^{19}\,cm^{-3}$) significantly increase the photoetch rate of the "host" HVPE material ($n = 10^{17}\,cm^{-3}$). The extent of the increase is determined by the ratio of the areas of the high and low-doped GaN exposed to solution and can be explained in terms of current (etch rate)–potential curves. The consequences of such galvanic effects on defect revealing for quality control of crystals are considered.

References

[1] J.L. Weyher, J.J. Kelly, Defect-selective etching of semiconductors, in: G. Dhanaraj, K. Byrappa, V. Prasad, M. Dudley (Eds.), Springer-Verlag, Berlin Heidelberg, 2010, pp. 1453–1476 (Chapter G-43).
[2] Z.P. Huang, N. Geyer, P. Werner, J. de Boor, U. Gosele, Adv. Mater. 23 (2011) 285.
[3] D.H. van Dorp, S. Arnauts, D. Cuypers, J. Rip, F. Holsteyns, S. De Gendt, J.J. Kelly, ECS J. Solid State Sci. Technol. 3 (6) (2014) P179.
[4] J.J. Kelly, X.H. Xia, C.M.A. Ashruf, P.J. French, IEEE Sens. J. 1 (2001) 735.
[5] C.M.A. Ashruf, P.J. French, P.M. sarro, R. Kazinczi, X.H. Xia, J.J. Kelly, J. Micromech. Microeng. 10 (2000) 505.
[6] X.L. Li, Curr. Opin. Solid State Sci. 16 (2012) 71.
[7] J. van de Ven, H.J.P. Nabben, J. Electochem. Soc. 138 (1991) 3401.
[8] X.H. Xia, C.M.A. Ashruf, P.J. French, J.J. Kelly, Chem. Mater. 12 (2000) 1671.
[9] M.S. Minsky, M. White, E.L. Hu, Appl. Phys. Lett. 68 (1996) 1531.
[10] C. Youtsey, I. Adesida, L.T. Romano, G. Bulman, Appl. Phys. Lett. 72 (1998) 560.
[11] C. Youtsey, L.T. Romano, R.J. Molnar, I. Adesida, Appl. Phys. Lett. 74 (1999) 3537.
[12] J.A. Bardwell, I.G. Foulds, J.B. Webb, H. Tang, J. Fraser, S. Moisa, S.J. Roife, J. Electron. Mater. 28 (1999) L24.
[13] T.L. Williamson, D.J. Diaz, P.W. Bohn, R.J. Molnar, J. Vac. Sci. Technol. B 22 (2004) 925.
[14] J. van de Ven, J.J. Kelly, J. Electrochem. Soc. 148 (2001) G10.
[15] T. Wolff, M. Rapp, T. Rotter, Phys. Status Solidi (a) 201 (2004) 2067.
[16] J.A. Bardwell, J.B. Webb, H. Tang, J. Fraser, S. Moisa, J. Appl. Phys. 89 (2001) 4142.
[17] H. Maher, D.W. DiSanto, G. Soerensen, C.R. Bolognesi, H. Tang, J.B. Webb, Appl. Phys. Lett. 77 (2000) 3833.
[18] S. Yoshida, J. Cryst. Growth 181 (1997) 293.
[19] E. Harush, S. Brandon, J. Salzman, Y. Paz, Semicond. Sci. Technol. 17 (2002) 510.
[20] Bo Yang, Patrick Fay, J. Vac. Sci Technol. B 22 (2004) 1750.
[21] L. Macht, J.J. Kelly, J.L. Weyher, A. Grzegorczyk, P.K. Larsen, J. Cryst. Growth 273 (2005) 347.
[22] D.H. van Dorp, J.L. Weyher, M.R. Kooijman, J.J. Kelly, J. Electrochem. Soc. 156 (2009) D371.
[23] J.L. Weyher Lewandowska, J.J. Kelly, L. Konczewicz, B. Lucznik, J. Cryst. Growth 307 (2007) 298.
[24] C. Frigeri, J.L. Weyher, L. Zanotti, J. Electrochem. Soc. 136 (1989) 262.
[25] M. Bockowski, I. Grzegory, B. Lucznik, T. Sochacki, G. Nowak, B. Sadovyi, P. Strak, G. Kamler, E. Litwin-Staszewska, S. Porowski, J. Cyst. Growth 350 (2012) 5.
[26] M. Boćkowski, B. Lucznik, T. Sochacki, M. Amilusik, E. Litwin-Staszewska, R. Piotrzkowski, I. Grzegory, Proc. SPIE 862509 (2013) 1.
[27] J.L. Weyher, F.D. Tichelaar, D.H van Dorp, J.J. Kelly, A. Khachapuridze, J. Cryst. Growth 312 (2010) 2607.
[28] J.L. Weyher, B. Łucznik, I. Grzegory, J. Smalc-Koziorowska, T. Paskova, J. Cryst. Growth 312 (2010) 2611.
[29] J.L. Weyher, Cryst. Res. Technol. 47 (3) (2012) 333.
[30] J.L. Weyher, T. Sochacki, M. Amilusik, M. Fijałkowski, B. Łucznik, R. Jakieła, G. Staszczak, A. Nikolenko, V. Strelchuk, B. Sadovyi, M. Boćkowski, I. Grzegory, J. Cryst. Growth 403 (2014) 77.
[31] P.H.L. Notten, J.J. Kelly, J. Electrochem. Soc. 134 (1987) 444.
[32] J.L. Weyher, F.D. Tichelaar, H.W. Zandbergen, L. Macht, P.R. Hageman, J. Appl. Phys. 90 (2001) 6105.
[33] J.L. Weyher, I. Dzięcielewski, A. Kamińska, T. Roliński, G. Nowak, R. Hołyst, J. Appl. Phys. 112 (2012) 114327.
[34] T. Sochacki, Z. Bryan, M. Amilusik, M. Bobea, M. Fijalkowski, I. Bryan, B. Lucznik, R. Collazo, J.L. Weyher, R. Kucharski, I. Grzegory, M. Bockowski, Z. Sitar, J. Cryst. Growth 394 (2014) 55.